Title: Molecular profiling predicts meningioma recurrence and reveals loss of DREAM complex repression in aggressive tumors

Authors: Akash J. Patel[1,2], Ying-Wooi Wan[2,3*], Rami Al-Ouran[2,6], Jean-Pierre Revelli[2,3], Maria F. Cardenas[4], Mazen Oneissi[1,2], Liu Xi[4], Ali Jalali[1], John F. Magnotti[1], Donna M. Muzny[4], HarshaVardhan Doddapaneni[4], Sherly Sebastian[1], Kent A. Heck[5], J. Clay Goodman[5], Shankar P. Gopinath[1], Zhandong Liu[2,6], Ganesh Rao[7], Sharon E. Plon[3,6], Daniel Yoshor[1,8], David A. Wheeler[4], Huda Y. Zoghbi[2,4,8,9*], and Tiemo J. Klisch[2,3*]

Affiliations:

[1] Department of Neurosurgery, Baylor College of Medicine, Houston, TX

[2] Jan and Dan Duncan Neurological Research Institute, Texas Children's Hospital, Houston, TX

[3] Department of Molecular and Human Genetics, Baylor College of Medicine, Houston, TX

[4] Human Genome Sequencing Center, Department of Molecular and Human Genetics, Baylor College of Medicine, Houston, TX

[5] Department of Pathology, Baylor College of Medicine, Houston, TX

[6] Department of Pediatrics, Baylor College of Medicine, Houston, TX

[7] Department of Neurosurgery, University of Texas MD Anderson Cancer Center, Houston, TX

[8] Department of Neuroscience, Baylor College of Medicine, Houston, TX

[9] Howard Hughes Medical Institute, Baylor College of Medicine, Houston, TX

***To whom correspondence should be addressed:** Tiemo Klisch (klisch@bcm.edu); Ying-Wooi Wan (yingwoow@bcm.edu); Huda Zoghbi (hzoghbi@bcm.edu)

One sentence summary: A combination of clinical and genetic data reveals a molecular classification for meningioma that predicts which tumors will be most aggressive and suggests biological differences among tumor classes.

Abstract

Meningiomas account for roughly one-third of all primary brain tumors. Although typically benign, about 20% of meningiomas are aggressive, and despite the rigor of the current histopathological classification system, there remains considerable uncertainty in predicting tumor behavior. Here we analyzed 160 tumors from all three WHO grades (I-III) using clinical, gene expression and sequencing data. Unsupervised clustering analysis identified three molecular groups that reliably predicted clinical severity. These groups did not directly correlate with the WHO grading system, which would classify more than half of the tumors in the most aggressive molecular group as benign. Transcriptional and biochemical analyses revealed that aggressive meningiomas involve loss of the repressor function of the DREAM complex, resulting in cell cycle activation, and only tumors in this group tend to recur after full resection. These findings should improve our ability to predict recurrence and develop targeted treatments for these clinically challenging tumors.

Introduction

Meningiomas are the most common primary tumors of the brain and central nervous system[1,2], and they are most commonly benign (WHO grade I). Roughly 20% of meningiomas are atypical (grade II) or malignant (grade III), however, with a five-year recurrence rate of up to 41%[3–5]; such tumors require serial resections until they become inoperable, and the five-year survival rate can be as low as 35%[6]. At present, the WHO histopathological classification system does not reliably predict whether an individual meningioma will behave aggressively[7]. We clearly need a better understanding of meningioma biology in order to develop viable therapeutic alternatives to surgery and adjuvant radiation.

There are good reasons to believe that meningioma might be amenable to the sort of molecular profiling that has transformed the diagnosis and treatment of medulloblastoma, glioma, and many other cancers in recent years[8–11]. The first hint of an underlying genetic mechanism came from the observation that meningiomas frequently arise in the context of neurofibromatosis type 2 (NF2)[12]. In fact, half of sporadic meningiomas and a majority of higher-grade tumors involve loss of NF2 function or loss of heterozygosity of chromosome 22q, where *NF2* is located[13,14]. Several whole exome/genome sequencing studies on benign (grade I) tumors have identified recurrent somatic mutations in *TRAF7, KLF4, AKT1, SMO*, and *POLR2A*[15–17]. Harmanci et al. focused on primary atypical (grade II) meningiomas and found a majority have loss of *NF2* along with either genomic instability or *SMARCB1* mutations[13]; this combination of features was not able to completely separate atypical from benign tumors, but the addition of the top 25 most differentially expressed genes raised the prediction accuracy of the model to 91% for atypical tumors with a high or medium Ki-67 index. Bi et al. found that grade III tumors are less likely to have *TRAF7*, *KL4*, *AKT1*, or *SMO* mutations but more likely to show genomic instability (copy number variation or CNV)[18]. Vasudevan et al. sought targetable pathways in high-grade meningiomas and found that high *FOXM1* expression is associated with poor clinical outcomes[19].

All these studies demonstrate that molecular approaches yield important insights. Nevertheless, each relied on the existing WHO histopathological classification system rather than seeking a molecular means of discriminating tumor behaviors across all grades. Here, we use an unsupervised approach to analyze RNA sequencing (RNA-seq) and whole-exome sequencing (WES) data from 160 fresh-frozen grade I, II and III meningioma samples. Our analysis yielded three distinct subgroups of meningioma that correlate with clinical outcomes better than the WHO classification; it also revealed a molecular signature for the most aggressive tumors that provides biological insight into their etiology.

Results

Patient Demographics and Pathologic Characteristics

We analyzed 160 meningioma samples from 140 patients. Five patients had two tumors resected independently and nine patients had at least one recurrence. According to the WHO histopathological classification system for meningioma, 121 tumors were grade I (benign), 32 were grade II (atypical), and 7 were grade III (malignant). Female sex confers greater risk for meningioma[1], and our cohort reflected the expected proportions, with 90 (64%) female and 50 (36%) male subjects. The median age at the time of initial surgery for these patients was 60 years (range 21-81 years). Seventy-nine percent of patients underwent a gross total resection, twenty-two percent underwent a subtotal resection, and in one case the extent of resection was unknown. Patients had a median follow-up of 28 months (range 0-91 months). Twenty-four tumors (17%) had a local recurrence. The recurrence rate for WHO I grade tumors was 11%; grade II, 42%; and grade III, 83%. The patient characteristics and pathology of our cohort are presented in Table S1. None of the tumors in our discovery or independent validation set had been treated with adjuvant radiation prior to profiling. Five patients had had radiation as children (four for cancers and one for tinea capitis); these are marked with an asterisk in Table S1.

Identification of Meningioma Subgroups by Transcriptome Analysis

To determine whether meningiomas could be differentiated based on gene expression profiles, we used principal component analysis (PCA) on a discovery set of 97 tumors (77 WHO grade I, 20 WHO grade II). The tumors did not cluster into distinct groups based on WHO grade (Fig. 1A).

We then employed non-negative matrix factorization (NMF) clustering for k=2 to k=7 using the 1,500 genes that varied most among the tumor samples. After 1,000 iterations, three clusters (k=3) emerged as providing the best fit as determined by the consensus membership, cophenetic and silhouette scores (Figure 1B, Figure S1A-C). The three distinct groups can also be discerned from the expression heatmap (Figure S1D). The three groups exhibit significant differences in WHO grade representation (p-value=0.0020, ANOVA): group 1 (green) is populated exclusively with WHO grade I tumors; group 2 (blue) contains mostly WHO grade I (79%) tumors, with 21% grade II; and the third group (red) contains similar proportions of WHO grade I and II tumors (56% and 44%, respectively; Table S1). Because the WHO grade III tumors in our cohort were all recurrences, they were not included in the primary transcriptome analysis.

We next analyzed two independent datasets: an independent cohort of 48 tumors (39 WHO grade I and 9 WHO grade II) and a published microarray dataset of 96 meningiomas[16]. First, we identified all genes that are common across all three datasets. We then performed pairwise comparisons between groups to identify those genes that were differentially expressed with a minimum fold-change of 1.5, at a false discovery rate of 1%. This yielded 3,484 genes, which we used to build a Random Forest classifier to predict groups in the two

validation sets. The expression pattern of this gene set in each group, as visualized in heat maps (Figure 1D), is very similar across the discovery and both validation datasets. These results provide evidence that the expression groups designated by differential gene expression of our discovery set are stable, even across platforms.

Next, we analyzed the association of clinical variables within the three transcriptionally defined groups (from here we will refer to our three molecular classes as groups 1, 2, and 3, as distinct from the WHO classification system's grades I, II, and III). One important clinical variable is the MIB1 index, a measure of the mitotic activity of the tumor, which has prognostic significance[18]. The median MIB1 index tracked with molecular group, being lowest in the first group, intermediate in the second, and highest in the third (2.5, 3.5, and 6.3, respectively; Figure 2A upper panel, p-value=0.0026, ANOVA), despite 56% of our group 3 tumors being WHO grade I. While the sample size is smaller in our validation cohort, we observed the same trend (Figure 2A, lower panel). To ensure that these differences were not due to a mixture of WHO grade tumors in the groups, we analyzed the MIB1 index of only the WHO grade I tumors (Figure 2B, left panels) and only the grade II tumors (Figure 2B, right panels) and found the same tracking of MIB1 index from molecular groups 1 to 3, within each WHO grade. Because the MIB1 index is based on Ki67 immunohistochemistry staining, which is subject to interobserver variability[19,20], we quantified the average transcript levels (MKI67) and observed a concordant result: statistically significant increases from molecular groups 1 to 3 in our discovery cohort (p-value<0.0001; Figure S2A, upper panel) and an identical trend in our validation cohort (Figure S2A, lower panel).

It has been reported that tumors with different somatic mutations cluster to different intracranial regions (e.g., TRAF7 and SMO mutant tumors tend to form in the anterior skull base)[15]. We therefore asked whether any of our three molecularly-defined groups were associated with specific locations (Figure 2C and Table S1). Although the small sample size relative to the number of factors precludes making statistically significant conclusions, we used a generalized linear model (Poisson link function) analysis to compare the distribution of tumors for each expression group across 16 anatomical locations. Only the anterior skull base and occipital locations showed a significant ($p<0.05$) difference between groups (adjusted $p = 0.0004$ and 0.0329, respectively) with group 1 tumors more likely to be located in the anterior skull base and group 3 tumors more likely to arise in the occipital region (Figure 2C).

We also examined the gender distribution in our expression groups. In our discovery set, groups 1 and 2 show the expected 2:1 female to male distribution, but 56% of patients in group 3 are male (p-value 0.0240, Table S1).

Lastly, we assessed the recurrence-free survival (RFS) across the three molecularly-defined groups (Figure 3). We first analyzed our discovery set of 97 tumors. WHO grade II tumors tend to have a worse RFS than WHO grade I tumors but this trend does not quite reach significance (Figure 3A left panel; log-rank p-

value=0.053, ANOVA). On the other hand, our group 1 and 2 tumors had an indistinguishable, low RFS with only four recurrences, even though 21% of the group 2 tumors would be classified by the current WHO grading system as "high grade." Group 3 tumors, however, have a significantly worse RFS than the two other groups (Figure 3A right panel; log-rank p-value<0.001, ANOVA), despite the fact that the majority of the tumors in group 3 are WHO grade I.

To ensure that the extent of resection was not responsible for these RFS differences, we looked at RFS for only those tumors that underwent gross-total resection. Both WHO grade I and II had recurrences, with more for WHO grade II (Figure 3B, left panel, p-value=0.02, ANOVA), but only group 3 tumors recurred in our molecularly-defined classification (Figure 3B, right panel, p-value<0.001, ANOVA).

To rule out the effect of WHO grade on the recurrence trends seen with our groups, we analyzed the RFS of our groups within each WHO grade in our discovery cohort (similar to our MIB1 analysis). We found that group 3 WHO grade I tumors have much worse recurrence rates (33%) than group 1 (8.6%) or group 2 (4.2%) WHO grade I tumors or WHO grade I tumors as a whole (13%) (p-value = 0.0018, ANOVA; Figure 3C, right panel). The same holds true within WHO grade II tumors (p-value 0.09, ANOVA; Figure 3C, left panel): group 3 WHO grade II tumors have a 57% recurrence rate, higher than group 2 (16.7% recurrence rate) or all WHO grade II tumors (45% recurrence rate).

Thus, our expression-based classification identifies WHO grade I/II tumors that have a high risk of recurrence. These data also suggest that total resection is less likely to cure group 3 tumors.

Copy Number and Somatic Alterations in Meningiomas

Since high-grade meningiomas have more chromosomal abnormalities[13,21], we analyzed the three groups of tumors for genomic instability using copy number data derived from whole-exome sequencing (WES) (Figure 4). We had copy number data for 84 tumors in the discovery cohort and 44 in the validation cohort. Group 1 had no notable chromosomal losses or gains. Group 2 tumors showed significant loss of chromosome 22q, the most commonly reported chromosomal abnormality in meningioma[22] (84%; p-value<0.0001, Chi-square); Figure 4A). Group 3 manifested the most genomic instability, showing loss of chromosome 22q (89%; p-value<0.0001 Chi-square) and chromosome 1p (79%; p-value<$1x10^{-5}$, Chi-square), the second most common reported abnormality[22,23]. Furthermore, over 20% of the group 3 tumors showed losses in chr3p, chr4p, chr6q, chr14p, chr14q, or chr18q (Figure 4A upper panel). Both validation sets replicated these results (Figure 4A, lower panels). Interestingly, loss of neither chr1p or chr22q, loss of only chr22q, and loss of both chr22q and chr1p are almost sufficient to distinguish between groups 1, 2, and 3, respectively. Combining all data sets, having neither chr1p or chr22q loss had a 94% sensitivity and 86% specificity with a positive predictive value (PPV) of 86% and a negative predictive value (NPV) of 94% for identifying group 1. Having loss of only chr22q had a sensitivity of 76%, specificity of 95%, PPV of 83% and NPV of 92% for identifying group 2.

Having loss of both chr22q and chr1p had a sensitivity of 68%, specificity of 95%, PPV of 83% and NPV of 90% for identifying group 3. We also examined the distribution of chromosome loss by gender and did not find a significant difference between females and males (Figure 4B). However, we noticed that the ratio of female to male differed between groups: combining all data sets, group 1 has 78% female patients, group 2 has 77%, and group 3 only 51% (p-value=0.0008, Chi-square).

WES also revealed 3,094 somatic mutations in our discovery cohort with a median of 0.47 mutations per megabase, which did not differ between groups (Group 1, 0.44; Group 2, 0.40; Group 3, 0.52; p-value=0.4951). Specific mutations did, however, cluster according to group. Only group 1 tumors contained mutations in *TRAF7* (52%, 40% and 61% in the discovery, validation and external set, respectively; Figure 4B). Group 1 also contained the highest percentage of *KLF4* (26%, 10%, 30%) and *AKT1* (19%, 15%, 23%) mutations (Figure 4B). In contrast, NF2 mutations were seen only in groups 2 (68%, 50%, 50%) and 3 (54%, 21y%, 60%). Strikingly, these mutations were usually combined with a loss of the other allele on chromosome 22p. SMARCB1 mutations were primarily seen in group 2, especially in the external set.

As the prevalence of NF2 mutations did not differ between groups 2 and 3 (68% and 54%, respectively; p-value=0.2837, Chi-square), we next explored whether the degree of NF2 expression loss could distinguish tumors in these groups. Both groups have markedly reduced levels of NF2 expression compared to group 1 (Figure S2B, p-value<0.0001) but did not differ from one another in this regard (Figure S2B, p-value=0.14). Both showed typical loss of function variants (nonsense and frameshift) spanning the NF2 coding region (Figure 4B and Table S2).

In sum, group 1 is characterized by recurrent somatic mutations in *TRAF7, KLF4* and *AKT1* but lacks any significant chromosomal gains/losses. Group 2 is characterized primarily by mutation in NF2 and loss of chr22q, and group 3 meningiomas have a significant burden of chromosomal gains/losses, most commonly loss of chr22q and chr1p together. Like WHO grade II and III tumors[24], our group 3 has a roughly equal proportion of females and males.

Gene Set Enrichment Analysis Further Distinguishes Groups 2 and 3

To better differentiate groups 2 and 3 and understand the biological pathways driving these tumors, we performed gene set enrichment analysis (GSEA)[25,26] for each expression group using the genes highly expressed in that group (Table S3). No single underlying pathway emerged for group 1 (Table S4). Four out of the five enriched categories in group 2 suggest that these tumors have lost the repressive activity of the PRC2 methyltransferase complex (Table S4). Genes highly overexpressed only in group 3 clustered in cell cycle modules, especially the G2/M checkpoint, which is regulated by the repressive transcription factors of the E2F family, such as E2F4, and its associated repressor, the DREAM complex[27]. The two modules, “genes with promoters bound by E2F4” and “targets of the DREAM complex” were the most enriched modules (Table S4).

To determine whether these two repressor complexes truly reflect biological differences between these groups of tumors, we evaluated the enrichment scores of their target genes in all three groups (Figures 5A). Strikingly, the expression pattern of these gene sets in group 2 is opposite that of group 3: the former is characterized by the loss or dysfunction of the repressive PRC2 complex, whereas the latter is characterized by loss or dysfunction of the repressive DREAM complex.

Loss of the PRC2 Complex in Group 2

The PRC2 complex is responsible for H3K27 di- and trimethylation and subsequent chromatin silencing. The core subunit consists of EED, SUZ12 and EZH1 or EZH2. We hypothesized that this complex is not forming in group 2 tumors, resulting in upregulation of the PRC2 target genes, as identified by the unbiased expression clustering. Therefore, we used cellular lysates from five tumors of each group, and immunoprecipitated the PRC2 complex using EZH1 (Figure 5B). All tested proteins were expressed in all tumors (Figure 5B, lysate lanes). Both EED and SUZ12 were detected in the EZH1 immunoprecipitates of group 1 and 3 tumors, but not group 2 tumors. This strongly suggests that the core complex is formed in group 1 and 3 tumors but not in group 2 tumors. Consistent with this finding, the PRC2 complex's direct targets, the HOX transcription factors[28,29], were significantly enriched only in group 2 (Figure 5C, q-value<0.001).

To clarify whether loss of the PRC2 complex drives the transcriptional dysregulation seen in group 2, we transfected 293t cells with either wildtype EZH1 (1-747aa) or SET domain–depleted Ezh1[30] (EZH1-ΔSET, 1-512aa, Figure 5D). The SET domain of EZH1 is responsible for the lysine-specific histone methyltransferase activity; without this domain, PRC2 cannot perform H3K27 methylation, and thus results in aberrant gene activation[31,32]. After 48 hours of over-expression, we performed qRT-PCR analysis of fifteen genes that were all significantly upregulated in group 2. We chose to include known PRC2 target genes (RBP4, ELN, CTGF, SFRP4, EPHB3, ATOH8)[33], including those which are also homeobox genes (NKX6.1, HOXB2, MKX)[33] (Table S3). We found all except one of these genes significantly upregulated in cells overexpressing EZH1-ΔSET compared to wild-type EZH1 (Figure 5D). Because meningiomas arise from arachnoid cap cells, we also generated an immortalized cell line from arachnoid cells (see methods for cell line establishment). As with the 293t cell line, the tested genes were upregulated upon loss of PRC2 complex function (Figure 5D).

In sum, group 2 meningioma appear to be driven by loss of PRC2 complex function.

Loss of the DREAM Complex in Group 3

The DREAM complex is a highly-conserved master regulator of the cell cycle[27]. It consists of MuvB core proteins: Lin52, Lin9, Lin37, Lin54 and RBBP4. When this core is bound to RB-like proteins (RBL1/2) and E2F, it forms the repressive DREAM complex, which keeps the cell quiescent. When the core associates with MYBL2 and FOXM1, however, it forms the activating DREAM complex, which allows cell cycle

progression and subsequent proliferation. Interestingly, tumors from group 3 have the highest proliferation index, and a recent study found elevated expression of FOXM1 associated with high-grade meningiomas[13,34].

We found increased expression of both FOXM1 and MYBL2 in our group 3 tumors, which aligns with our previous results suggesting that the DREAM complex has lost its repressive activity and allowed upregulation of these two target genes. To confirm that group 2 and group 3 tumors differ in the form of the DREAM complex that they express, we immunoprecipitated the core complex in tumors from all three groups using Lin37. All investigated proteins were expressed in all tumors (Figure 5B, lysate lanes), but RBL2 was associated with the core only in group 1 and 2 tumors (Figure 5B). On the other hand, only in group 3 tumors was the core associated with both FOXM1 and MYBL2. Thus groups 1 and 2 contain the repressive form of the DREAM complex, whereas group 3 tumors contain the activator forms of the complex.

If this is indeed the case, we would expect to see increased expression of DREAM target genes in group 3 tumors and decreased levels in the other two groups. GSEA revealed that known DREAM target genes are highly enriched only in group 3 tumors (Figure 5C, q-value<0.001). Using a strategy similar to that used for group 2 and the PRC2 complex, we took advantage of recently published dominant-negative forms of two MuvB core members, Lin37[35] and Lin52[36]. It has been shown that mutation in two small domains in Lin37 (CD1 and CD2) results in the loss of the repressive function of the DREAM complex (Lin37-WT (1-243aa) and Lin37-DN),[35] and inhibiting phosphorylation of Serine28 on Lin52 results in similar phenotypes (Lin52-WT (1-116) and Lin52-DN)[36]. We performed qRT-PCR analysis of fourteen genes that were all significantly upregulated in group 3, some of which were known DREAM targets (MYBL2, FOXM1, TTK, PBK, MELK, and CDK1)[37]. Overexpression of both dominant-negative constructs resulted in the upregulation of these genes in both 293t cells (Figure 5D) and our arachnoid cell line (Figure 5D).

In sum, group 3 meningioma appear to be driven by loss of the repressive DREAM complex function.

Recurrent Tumors Match the Gene Expression Profile of the Original Tumor

Nine patients in our cohort had at least one resected recurrence with tissue available; two of these patients had multiple recurrences. Tumor progression was seen in three patients with group 1 tumors who could not have a complete resection due to tumor location. Gene expression profiling of these recurrent tumors demonstrated that they all remained within the group of the original tumor (Figure 6). Interestingly, three patients with group 3 tumors started with WHO grade II tumors that progressed to WHO grade III tumors, but their expression profile never changed. Three patients with WHO grade I tumors had inexplicably rapid recurrences, despite complete resection in one; both of their primary and recurrent tumors fell into expression group 3. Together, these data highlight the consistency of the molecular classification in predicting recurrences.

Discussion

The current histopathologic system for classifying meningiomas has shown some ability to predict clinical course, with WHO grade II and III tumors generally showing worse outcomes. Yet a subset of grade I tumors recur, despite successful resection and the appearance of benign features. Here we used unsupervised gene expression clustering of RNA-seq data from a large cohort of meningioma tumors from all three grades to define new groups that better correlate with two important outcome measures: proliferation as measured by MIB1 index and recurrence-free survival. Most importantly, our expression-based model can identify WHO grade I tumors that are at high risk for recurrence. For example, one of the patients in our clinic whose tumors are profiled in this study had total resection of a grade I tumor that recurred two years later; complete resection of this second tumor, also grade I, was insufficient to prevent a second recurrence 18 months later—still grade I, although the mitotic index had risen to 9.1. Our molecular classification, however, identified the tumors as belonging to group 3.

This is the major difference between our study and previous explorations of the genomic landscape of meningioma, which maintained the framework of the existing WHO histopathological classification[13,15–17,21,34,38]. For example, one study of atypical (grade II) tumors found the majority to have NF2/chr22q loss and genomic instability along with overexpression of the E2F2 and FOXM1 transcriptional networks[13]. Another study of high-grade tumors found overexpression of FOXM1 to be associated with poor clinical outcome[34]. Only by including the whole spectrum of tumor grades, gender and age in our cohort were we able to distinguish the very different biology of group 2 and 3 tumors: we showed that loss of the PRC2 complex underlies group 2 pathogenesis, whereas loss of the repressive function of the DREAM complex accounts for FOXM1 overexpression in group 3 tumors.

The pressing need in the meningioma field is to understand the biology that differentiates aggressive meningiomas from less aggressive ones so that we may start dissecting the pathways that drive pathogenesis and establish the first step towards developing adjuvant therapies.

Salient features of groups 1, 2, and 3

In our cohort, group 1 tumors were characterized by mutations in *TRAF7*, *KLF4*, and *AKT,* which confirms previous observations in benign meningiomas[15,17]. It is possible that the downstream consequences of these mutations converge biologically.

In our group 2 tumors, 91% showed loss of chromosome 22q. Our data suggest that these tumors lose PRC2 complex function and follow a more benign clinical course: their recurrence rate is as low as that of group 1 tumors, i.e., extremely rare if the tumor was resected completely.

Group 3 tumors appear to be driven instead by the activator forms of the DREAM complex and subsequent upregulation of its target genes, including MYBL2 and FOXM1. Elevated FOXM1 levels were

recently reported in aggressive meningiomas[34] (as well as other cancers[27]), but our findings suggest that this upregulation is secondary to the loss of DREAM complex-mediated repression. Our findings suggest that FOXM1 and MYBL2 act as co-activators of the DREAM complex rather than as independent transcription factors.

Of note, 79% of group 3 tumors showed loss of both 1p and 22q. All the WHO grade III tumors in our sample (which were all recurrences) show this double loss, but two of the original tumors were classified as WHO grade I. Our molecular classification, by contrast, placed all these tumors in group 3. These data suggest that testing for loss of even just these two chromosomes could provide a valuable biomarker for high-grade meningioma. That our group 3 tumors, the most aggressive group, consisted of a mixture of WHO grade I and II underscores the importance of developing robust molecular profiles to supplement histopathology.

In summary, our three molecular groups differ clinically and biologically, and predicted clinical course better than the WHO classification. In terms of clinical application, it would be costly to perform transcriptomic analysis on an individual tumor; much larger cohorts will be needed to narrow down the 3,484 genes to a more streamlined genetic signature. Moreover, our findings need to be confirmed with follow-up periods longer than 5 years, because many of these tumors have such an indolent course. In short, larger scale studies will be needed to confirm our observations to better understand meningioma biology and improve prognostication of these most difficult tumors.

Methods

Data reporting

No statistical methods were used to predetermine sample size. The experiments were not randomized, and the investigators were not blinded to allocation during experiments and outcome assessment.

Sample Selection and Preparation

We obtained primary tumor tissue (fresh frozen) from 157 meningiomas in 143 patients who were treated at Baylor College of Medicine (BCM). All patients provided written informed consent, and tumor tissues were collected under an IRB approved protocol at BCM. All meningiomas were initially signed out by one of two neuropathologists (K.H. or J.C.G.) and were graded based on the 2016 WHO guidelines. Mitotic index (MIB1) was calculated by determining the percentage of meningioma cell nuclei positive for Ki-67 staining. We used blood DNA as a reference for detecting somatic tumor mutations. We performed RNA sequencing on 166 tumors. One tumor sample was noted to have a NAB2-STAT6 gene fusion, that, based on the 2016 WHO guidelines[39], is now diagnostic for hemangiopericytoma/solitary fibrous tumor. Upon independent review by our neuropathologist, the patient was excluded from our analysis. We thus analyzed 160 meningiomas from 140 patients; 121 benign (WHO grade I), 32 atypical (WHO grade II) and 7 malignant (WHO grade III)

meningiomas. One-hundred and twenty-eight of these samples had adequate DNA for whole-exome sequencing. Only representative fresh-frozen blocks with estimated purity of ≥95% were selected for DNA and RNA extraction from 20-30 mg of tumor tissue using TRIzol (Thermo Fisher Scientific, MA) according to the manufacturer's protocol. Normal DNA was extracted from 1 ml of whole blood stored in PAXgene blood DNA tubes using the PAXgene Blood DNA Extraction Kit (Qiagen, CA) according to the manufacturer's protocol.

Patient Data Review

Under the aegis of a BCM IRB-approved protocol, we reviewed the following data: patient age at surgery, gender, race, tumor size, tumor location and extent of resection, histologic grade by WHO guidelines, and mitotic index (MIB1 index). Diagnostic imaging was re-reviewed to define tumor location, extent of resection and presence/date of local recurrence. Local recurrence after gross total resection was defined as local development of any contrast enhancement on subsequent brain imaging. Local recurrence after subtotal resection was defined as measurable growth of residual tumor. Vital status of the patient was obtained from search of the electronic medical record. A summary of clinical information is available in Table 1.

Next generation sequencing and analysis

All protocols and analyses were performed by the Human Genome Sequencing Center of Baylor College of Medicine (BCM-HGSC, https://www.hgsc.bcm.edu) according to their standard operation procedures.

DNA sequencing

DNA libraries were constructed according to the manufacturer's protocol with modifications. Briefly, 0.5 μg DNA was sheared into fragments of 200–300 base pairs in a Covaris plate with E210 system (Covaris, MA) followed by end-repair, A-tailing and ligation of Illumina multiplexing PE adaptors. Pre-capture Ligation Mediated-PCR (LM-PCR) was performed using the Library Amplification Readymix containing KAPA HiFi DNA Polymerase (Kapa Biosystems, MA). Universal primer IMUX-P1.0 and IMUX-P3.0 were used in PCR amplification. Purification was performed with Agencourt AMPure XP beads (Beckman Coulter, CA) after enzymatic reactions. Following the final XP beads purification, quantification and size distribution of the pre-capture LMPCR product was determined using the LabChip GX electrophoresis system (PerkinElmer, MA) and gel analysis using AlphaView SA v3.4 software. For exome capture, four pre-capture libraries were pooled together. The pooled libraries were then hybridized in solution to the HGSC VCRome 2.1 design (42Mb, Roche NimbleGen, WI). Post-capture LM-PCR amplification was performed using the Phusion High-Fidelity PCR Master Mix. After the final AMPure XP bead purification, quantity and size of the capture library was analyzed using the Caliper LabChip GX electrophoresis system. The efficiency of the capture was evaluated by performing a qPCR-based quality check on the enrichment level of four standard NimbleGen control loci. All

sequencing runs were performed in PE mode on Illumina HiSeq2000 platform.

Bioinformatics analyses for whole exome-sequencing data

Initial sequence analysis was performed using the HGSC Mercury analysis pipeline, from which the sequence reads of each sample were mapped to GRCh37 Human reference genome using the Burrows-Wheeler aligner (BWA, RRID:SCR_010910) and then recalibrated and realigned by GATK (RRID:SCR_001876). Mutations called by BCM-HGSC were generated by the standard cancer analysis pipeline, CARNAC (Consensus and Repeatable Nucleotide Alterations in Cancer), as described previously[40,41].

RNA sequencing

Genomic RNA was quantified by Picogreen (Thermo Fisher Scientific, MA) and its quality was assessed using a 2100 Bioanalyzer (Agilent, CA). RNA was selected for sequencing only if the RIN value was >6. RNA samples (1 μg) were fragmented, converted into double-stranded cDNA and then proceeded to library prep using TrueSeq RNA Sample Preparation (Illumina, San Diego, CA) according to the manufacturer protocol using a 15-cycle amplification. After PCR primers removal using Agencourt AMPure PCR Purification kit (Beckman Coulter, CA), the libraries were analyzed and quantified on TapeStation (TapeStation Instrument, RRID:SCR_014994) using the DNA High Sensitivity kit (Agilent, CA) to verify correct fragment size and to ensure the absence of extra bands. Equimolar amounts of DNA were pooled for capture (8 samples per pool) and verified by TapeStation. The captured libraries were sequenced on a HiSeq 4000 (Illumina HiSeq 4000 System, RRID:SCR_016386) on a version 3 TruSeq paired end flowcell according to manufacturer's instructions at a cluster density between 700 and 1000 K clusters/mm^2. The resulting BCL files containing the sequence data were converted into ".fastq.gz" files and individual libraries within the samples were demultiplexed using CASAVA 1.8.2 (CASAVA, RRID:SCR_001802) with no mismatches. All regions were covered by >20 reads.

Bioinformatics analyses for RNA sequencing data

Raw reads from the RNA-seq samples were processed using an in-house pipeline that uses TopHat2 (RRID:SCR_013035) for read alignment; FastQC (RRID:SCR_014583) and RSeQC (RRID:SCR_005275) for read and alignment quality assessment; HTSeq (RRID:SCR_005514) for expression count; and GATK (RRID:SCR_001876) for variant calling. The reads were aligned to GRCh37 human reference genome and mapped to the human transcriptome according to UCSC gene annotations. The RNA-seq read counts for genes were normalized and transformed into log-counts using the voom method (variance modeling at the observational level)[42] implemented in R package limma[43]. The normalized counts were then batched corrected using ComBat method implemented in R package sva[44]. Batch-corrected expression data were used for

subsequent subtype analysis using R software package NMF (https://cran.r-project.org/web/packages/NMF/index.html). Expression heatmaps were generated using Pheatmap (RRID:SCR_016418). Differential gene expression analysis of genes between the risk groups identified was carried out using the limma package on batch-corrected expression data.

To compare the discovery set with the validation sets, a list of 3,484 genes that were expressed in all three data sets was identified. Using this gene set, we were able to compare the three subtypes in a pairwise manner and identified differentially expressed genes (FDR of 1% and fold change >= 1.5) using the limma package. To verify the gene signature in the validation datasets, we first transformed the gene counts in the training and validation datasets to z-scores. We then built a Random Forest classifier using the gene signature and used it to predict the subtype classes for the samples in the validation datasets. Heatmaps for the validation datasets were produced using the assigned labels from the RF and similar gene ordering as in the training dataset heatmap. Heatmaps were implemented using the R package pheatmap.

Statistical analysis

For all analyses, a p-value<0.05 was considered significant. Recurrence-free survival (RFS) analysis and subsequent survival data visualization were carried out in R, using survival and survminer (https://CRAN.R-project.org/package=survminer) packages, respectively. ANOVA and Chi-square tests were used to compare clinical variables between groups. We used R to fit a generalized linear model (GLM) with a poisson link function (R function glm) to compare the rates of tumors by group and location. Main effects and interactions were tested using an analysis of deviance (chi-square), provided by the car package (https://CRAN.R-project.org/package=car). After a significant group-by-location interaction, we used further chi-squares tests to determine group differences within each location. False discovery rate correction was used to account for Type I error inflation due to multiple comparisons (16 locations). To compare group-by-location patterns between our discovery and validation datasets, we used the Bayesian Information Criterion (BIC) to compare two GLMs: one GLM contained interactions with dataset, the other model contained only a main effect of dataset (to account for differences in sample size). The model with the lower BIC provides the better fit to the data, with a BIC difference of 10 used as a threshold for decisive evidence in favor of a given model.

Gene Set Enrichment Analyses

One over-expressed gene list per risk group was generated using RNA-seq expression data that had a logFoldChange >1 with a false discovery rate <0.001 (Table S3). Gene Set Enrichment Analyses (GSEA, RRID:SCR_003199) were performed as described elsewhere[25] using curated gene sets (C2). All gene sets with an overlap of 15% or more percent were considered in the analysis and can be found in Table S4. The following

gene sets from the Broad Institute (https://software.broadinstitute.org/gsea/) were used: PRC2 target genes (combination of M9898, M7617, M8448), DREAM target genes (M149), Cell cycle genes (M7963). The HOX genes that are known to be repressed by the PRC2 complex were generated by identifying the intersection the homeodomain proteins[45] with the following GSEA gene lists: M7617, M10371, M1938, M8448, M9898. This identified 163 HOX genes.

Antibodies

Western blot (overnight incubation with a 1:5,000 dilution): anti-EED (chicken, GTX14294, GeneTex, TX), anti-SUZ12 (D39F6, rabbit, 3737S, Cell Signaling Technology, MA), anti-Vinculin (hVIN, mouse, V9131, MilliporeSigma, MA), anti-FOXM1 (rabbit, GTX102126, GeneTex, TX), anti-MYBL2 (rabbit, GTX77893, GeneTex, TX), anti-RBL2 (D9T7M, rabbit, 13610, Cell Signaling Technology, MA), anti-Mouse-HRP (1:50:000, 715-035-150, Jackson ImmunoResearch Labs, PA, RRID:AB_2340770), anti-Rabbit-HRP (1:20,000, 170–5046 Bio-Rad/AbD Serotec, CA, RRID:AB_11125757), anti-Chicken-HRP (1:2,000, NBP1-74785, Novus Biologicals, CO). Co-IP: anti-EZH1 (rabbit, 2 µg per IP, GTX108013, GeneTex, TX), anti-LIN37 (rabbit, 5 µg per IP, GTX44925, GeneTex, TX).

Co-Immunoprecipitation

PRC2 immunoprecipitations were carried out with 10 mg of tissue in 200 µl of PRC2 lysis buffer [50 mM HEPES (pH 7.0), 250 mM NaCl, 0.1% Nonidet P-40, 5 mM EDTA, freshly added: 0.5 mM dithiothreitol, 1 mM PMSF, 1X Xpert Phosphatase Inhibitor and 1X Xpert Protease Inhibitor Cocktail (P3200 and P3100, GenDEPOT, TX)]. DREAM immunoprecipitations were carried out with 50 mg of tissue in 200 µl of DREAM lysis buffer [20 mM Tris (pH 7.5), 420 mM NaCl, 1.5 mM MgCl2, 1 mM EDTA, 5% glycerol, freshly added: 1 mM dithiothreitol, 1 mM PMSF, 1X Xpert Phosphatase Inhibitor and 1X Xpert Protease Inhibitor Cocktail (P3200 and P3100, GenDEPOT, TX)]. After tissue disruption via sonication (three rounds with 3, 4 and 5 pulses respectively at 20% duty cycle), lysates were cleared via centrifugation for 20 minutes at 21,000 RCF at 4°C and transferred to siliconized tubes. The antibody was added and after a 2-hour incubation at 4°C on a rotor, 40 µl of agarose beads were added for another 30 minutes. Antibody-bead complexes were washed five times in their respective buffers and subject to standard western blot analysis using 1% input and 50% eluates.

Cell culture

Cell culture and qRT-PCR

Arachnoid cells were immortalized using a lentivirus harboring the SV40 large T antigen [pBABE-puro SV40 LT was a gift from Thomas Roberts (Addgene, RRID:Addgene_13970) as previously described[46]. NF2 haplotype was validated using qRT-PCR using a dilution series of DNA from 293T (NF2 wildtype) and

arachnoid cells. 293T cell line was purchased from ATCC (CRL-3216, Manassas, VA). Cells were found to be negative for mycoplasma contamination. Cell lines were cultured as adherent cells in DMEM containing 10% FBS and antibiotics using standard cell culture practices (Geraghty et al., 2014). 293T or arachnoid cells were transfected using Lipofectamine 3000 (Thermo Fioscher, Carlsbad, CA)using the following constructs: hEZH1-GFPpcDNA3 (aa1-747), EZH1_deltaSET-GFPpcDNA3 (aa1-512), hLIN37-GFPpcDNA3 (aa1-243), hLIN37_CD1/2-GFPpcDNA3 (aa1-243)[35], hLIN52-GFPpcDNA3 (1-116) and Lin52_S28A-GFPpcDNA3)[36].

After 48 hours of culture, total RNA was isolated using TRIzol, subject to reverse transcription and qRT-PCR. Primer information is available upon request.

Figures:

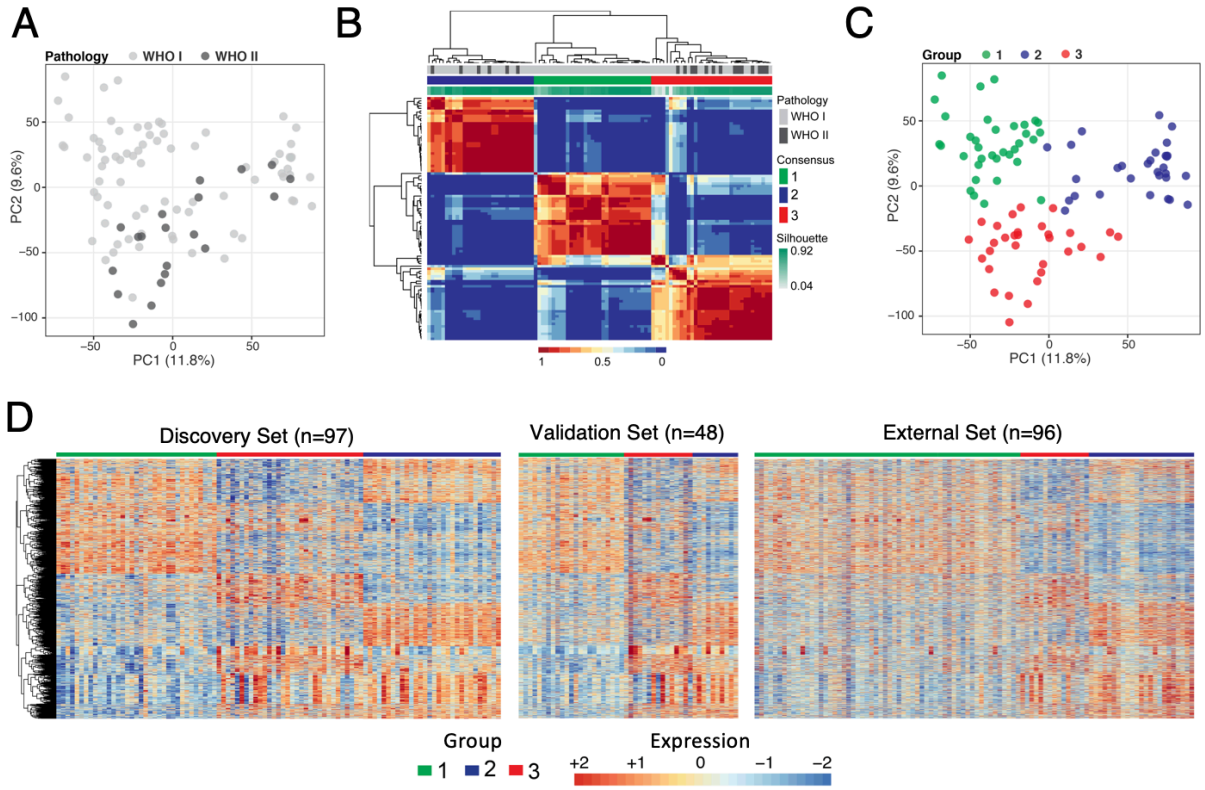

Fig. 1 Identification of meningioma subtypes using gene expression profiles. (**A**) Principal component analysis (PCA) on all genes of 97 tumors colored by WHO grading. WHO grade I tumors are represented by light grey circles; WHO grade II tumors are represented by dark grey circles. (**B**) Consensus matrix of the tumors for k=3 from 1000 runs of non-negative matrix factorization analysis depicts three distinguishable groups based on the gene expression data. (**C**) PCA on all genes, colored according to molecularly-defined groups. (**D**) Expression heatmap of the 3,484 genes common in all three data sets. The expression patterns of these genes distinguish three expression groups in our discovery set (left panel), validation set (middle panel) and publicly available data set (right panel). Group 1 is labelled in green; group 2, blue; group 3, red.

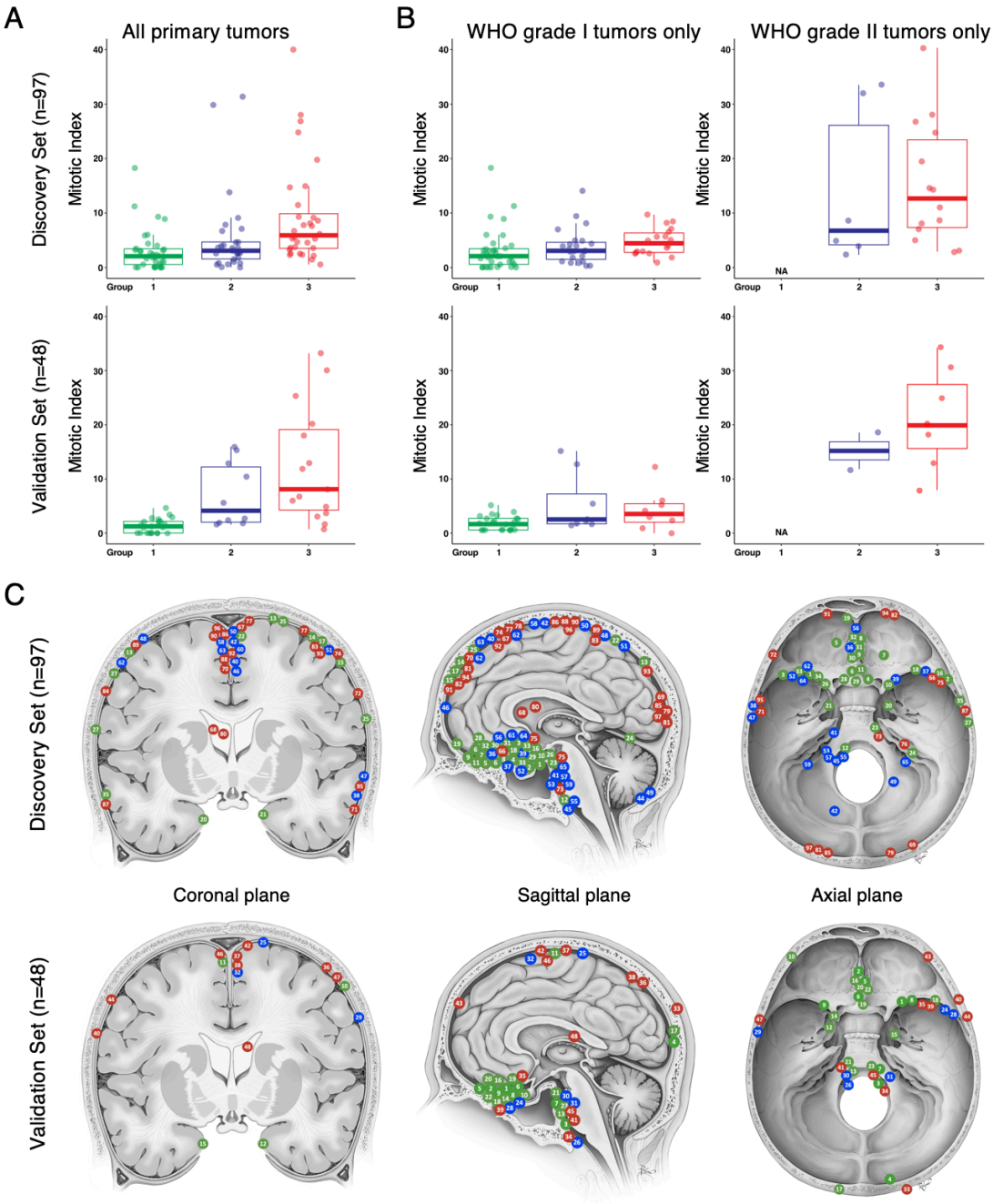

Fig. 2 Clinical characteristics of gene expression-defined meningioma groups. Group 1 is labelled in green; group 2, blue; group 3, red. (**A**) Boxplots showing the median mitotic index (MIB1) for groups 1 to 3 in the discovery set (p-value=0.0026, ANOVA, upper panel) and the validation set (p-value<0.0001, ANOVA, lower panel). (**B**) Boxplot of the MIB1 for groups 1 to 3 for only WHO grade I tumors (left panels) in the discovery set (p-value=0.4359, ANOVA, upper panel) and the validation set (p-value=0.0044, ANOVA, lower panel) and WHO grade II tumors (right panels) in the discovery set (p-value=0.6059, ANOVA, upper panel) and the validation set (p-value=0.3380, ANOVA, lower panel). (**C**) Location of tumors in our cohort in the discovery set (upper panels) and validation set (lower panels). Each tumor is marked on 2 views, either coronal and sagittal or axial and sagittal, respectively.

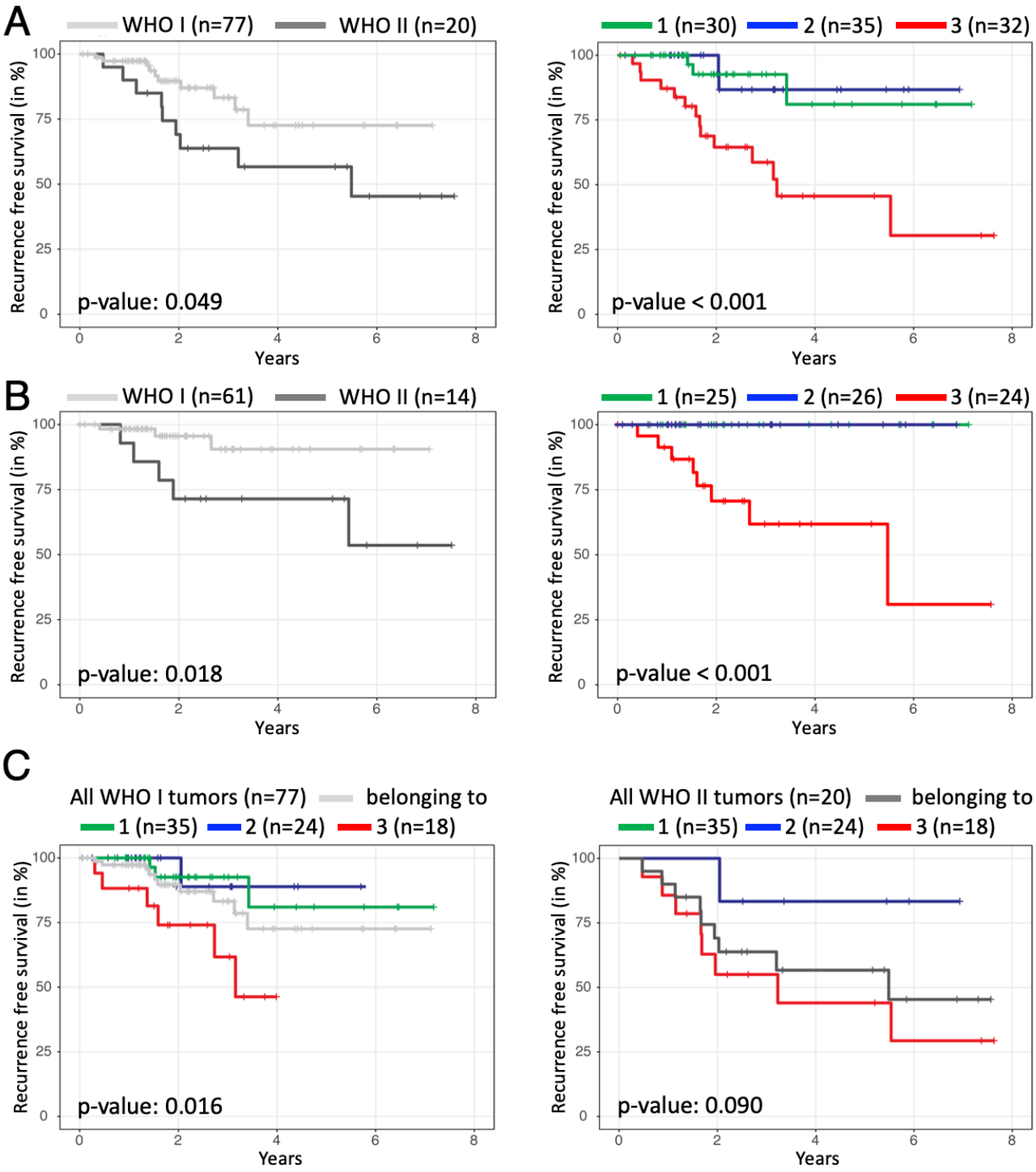

Fig. 3 Recurrence-free Survival of WHO grade and gene expression-defined meningioma groups. Recurrence-free survival analysis (RFS) based on (**A**) WHO grading (left panel) and by expression-defined subgroups (right panel) in all tumors and (**B**) only tumors that underwent complete resection. (**C**) RFS for expression-defined subgroups within only WHO grade I tumors (left panel) or WHO grade II tumors (right panel) shows the ability of the expression groups to refine RFS despite WHO grading. N represents the initial number of patients for each curve.

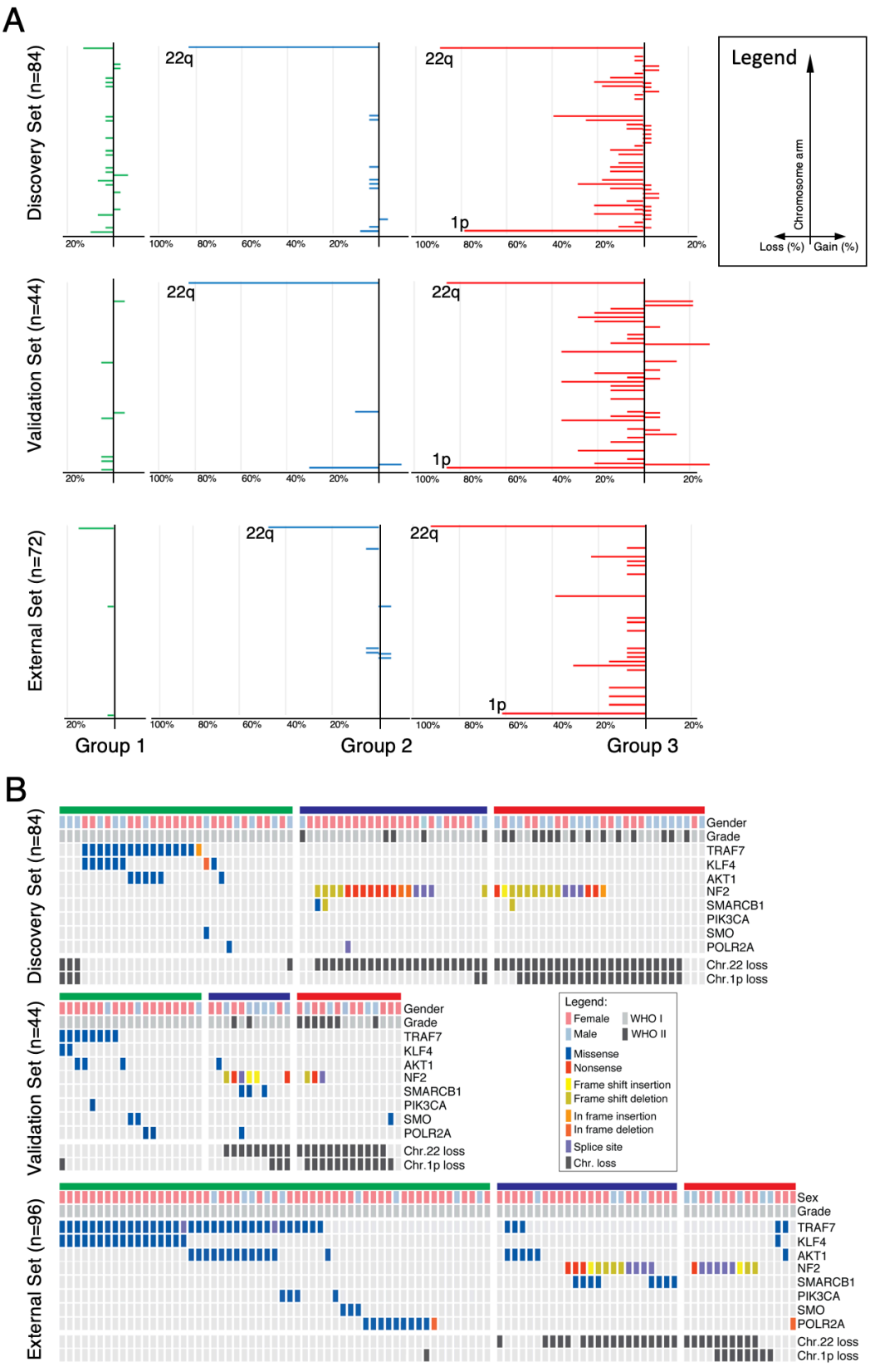

Fig. 4 Genomic landscape of meningiomas by gene expression-defined groups. Group 1 is labelled in green; group 2, blue; group 3, red. (**a**) Differences in chromosomal alterations by subgroup are shown with losses to the left and gains to the right. (**b**) Oncoprint depicting the mutation profiles of meningiomas in each expression group in the discovery set (upper panel) and the internal and external validation sets (lower panel).

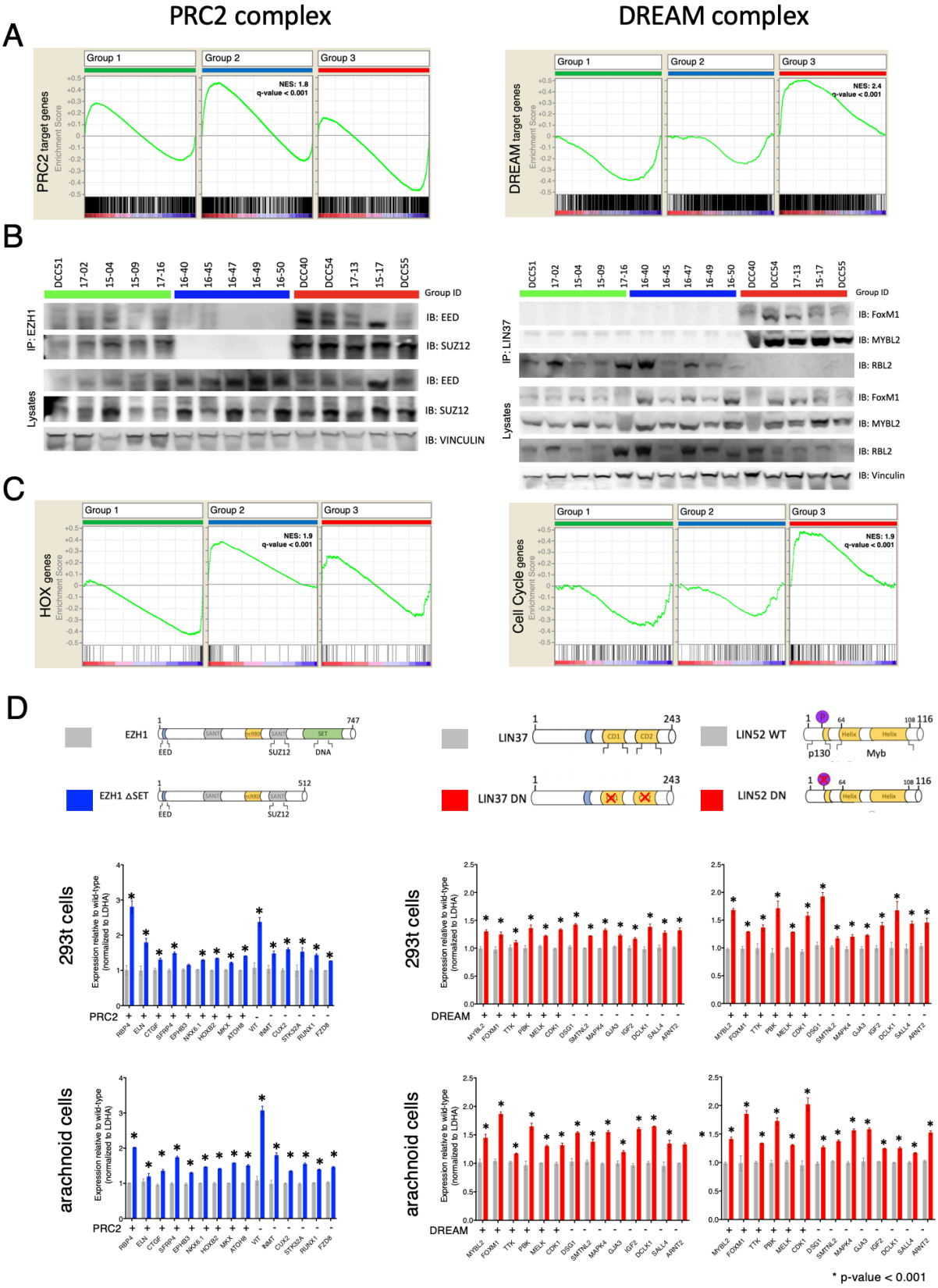

Fig. 5 Validation of PRC2 and DREAM complex disruption in group 2 and 3 tumors, respectively. (**A**) GSEA analysis of the PRC2 (left) and DREAM (right) target genes in each group. (**B**) *Left*: Co-immunoprecipitation studies using 5 tumors per group for EZH1 then probed for anti-EED and anti-SUZ12. *Right*: Co-immunoprecipitation studies using 5 tumors per group for Lin37 then probed for anti-FoxM1, anti-

MYBL2, and anti-RBL2. (**C**) GSEA analysis shows that HOX genes are enriched in group 2 (left) and cell cycle genes in group 3 (right). (**D**) qRT-PCR analysis measuring expression levels of group-specific upregulated genes and in 293t and arachnoid cells. *Left*: cells were transfected with either wild-type hEZH1 or hEZH1 ΔSET (dominant-negative EZH1). *Right*: cells were transfected with either wild-type hLIN37 or dominant-negative hLIN37 (left side) or either wild-type hLIN52 or dominant-negative hLIN52 (right side).

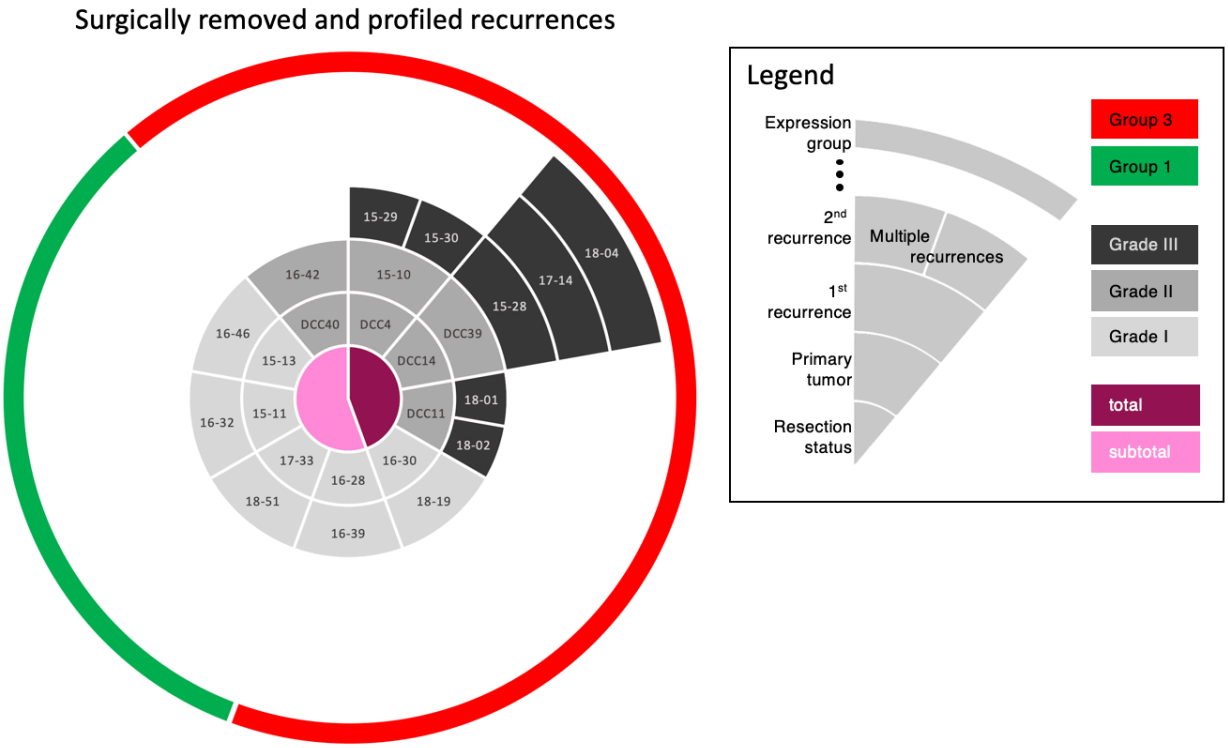

Fig. 7 Transcriptional Analysis of Tumor Recurrences. Expression profiling of recurrent tumors in our cohort demonstrates that the expression subtype is predictive when resection is complete, and remains unchanged between primary and recurrent tumors, unlike the WHO grading, which changes with disease progression.

Table overviews:

Table 1	Patient data
Table S1	Detailed tumor data
Table S2	NF2 mutations in discovery and validation sets
Table S3	Differentially expressed gene list
Table S4	GSEA analysis of expression groups

	Test Set (95 patients)					**Validation Set (47 patients)**			
Characteristic	**All Patients**	**Group 1 (no.=35)**	**Group 2 (no.=30)**	**Group 3 (no.=32)**	**p-value** btwn groups	**All Patients**	**Group 1 (no.=23)**	**Group 2 (no.=10)**	**Group 3 (no.=15)**
sex, no. of patients (%)									
male	36(38)	12(34)	7 (23)	18 (56)	**0.0240**	14 (30)	3(13)	6(60)	6(40)
Female	60(62)	23(66)	23 (77)	14 (44)		32 (70)	20(87)	4(40)	9(60)
median age (years) at surgery (range)	60(27-81)	62(33-79)	58.5 (27-81)	58.5 (33-78)	0.465	59 (18-81)	58 (21-78)	63.5 (26-81)	63 (18-77)
Location (%)									
Anterior Cranial Fossa	15(16)	13(37)	2(7)	0(0)	**4E-04**	7(15)	7(30)	0(0)	0(0)
Middle Cranial Fossa	2(2)	2(6)	0(0)	0(0)	0.193	2(4)	2(9)	0(0)	0(0)
Sphenoid Wing	16(16)	9(26)	5(17)	2(6)	0.193	9(19)	5(22)	2(20)	2(13)
Parafalcine	15(15)	1(3)	7(23)	7(22)	0.18	6(13)	1(4)	1(10)	4(27)
Petroclival	7(7)	1(3)	5(17)	1(3)	0.193	2(4)	2(9)	0(0)	0(0)
Clival	4(4)	1(3)	2(7)	1(3)	0.903	9(19)	3(13)	4(40)	2(13)
Frontal	14(14)	5(14)	1(3)	8(25)	0.1800	7(15)	1(4)	2(20)	4(27)
Occipital	5(5)	0(0)	0(0)	5(16)	**0.033**	2(4)	2(9)	0(0)	0(0)
Parietal	6(5)	1(3)	2(7)	3(9)	0.729	1(2)	0(0)	0(0)	1(7)
Temporal	6(6)	1(3)	2(7)	3(9)	0.729	0(0)	0(0)	0(0)	0(0)
Tentorial	1(1)	1(3)	0(0)	0(0)	0.485	0(0)	0(0)	0(0)	0(0)
Intraventricular	2(2)	0(0)	0(0)	2(6)	0.193	1(2)	0(0)	0(0)	1(7)
Cerebellum	2(2)	0(0)	2(7)	0(0)	0.193	0(0)	0(0)	0(0)	0(0)
Spine	2(2)	0(0)	2(7)	0(0)	0.193	1(2)	0(0)	1(10)	0(0)
WHO Grade (%)									
Grade I	77(79)	35(100)	24(80)	18(56)	**0.002**	39(81)	23(100)	8(80)	8(53)
Grade II	20(21)	0(0)	6(20)	14(44)		9(19)	0(0)	2(20)	7(47)
Median MIB1 Index (range)	3.1 (0.5-40)	2.5 (0.5-18.5)	3.5 (0.5-31.5)	6.3 (1-40)	**0.004**	2.6(1-32.7)	2.2 (1-5.5)	5 (2.5-16.5)	8.2 (1-32.7)
Extent of Resection (%)									
Gross Total Resection	76(79)	25(71)	27(90)	24(75)		38(79)	16(70)	9(90)	13(87)
Subtotal Resection	20(21)	10(29)	3(10)	7(22)	0.482	10(21)	7(30)	1(10)	2(13)
Unknown	1(1)	0(0)	0(0)	1(3)		0(0)	0(0)	0(0)	0(0)
Median Follow-up (months; range)	28 (0-91)	26 (8-86)	25 (1-83)	31 (0-91)	0.572	11.5 (0-20)	5 (0-17)	3 (0-17)	4 (0-20)
Death (%)	1(1)	0(0)	0(0)	1(3)	0.358	1(2)	0(0)	1(11)	0(0)

Table 1: Summary of Clinical Data of 140 patients with meningiomas.

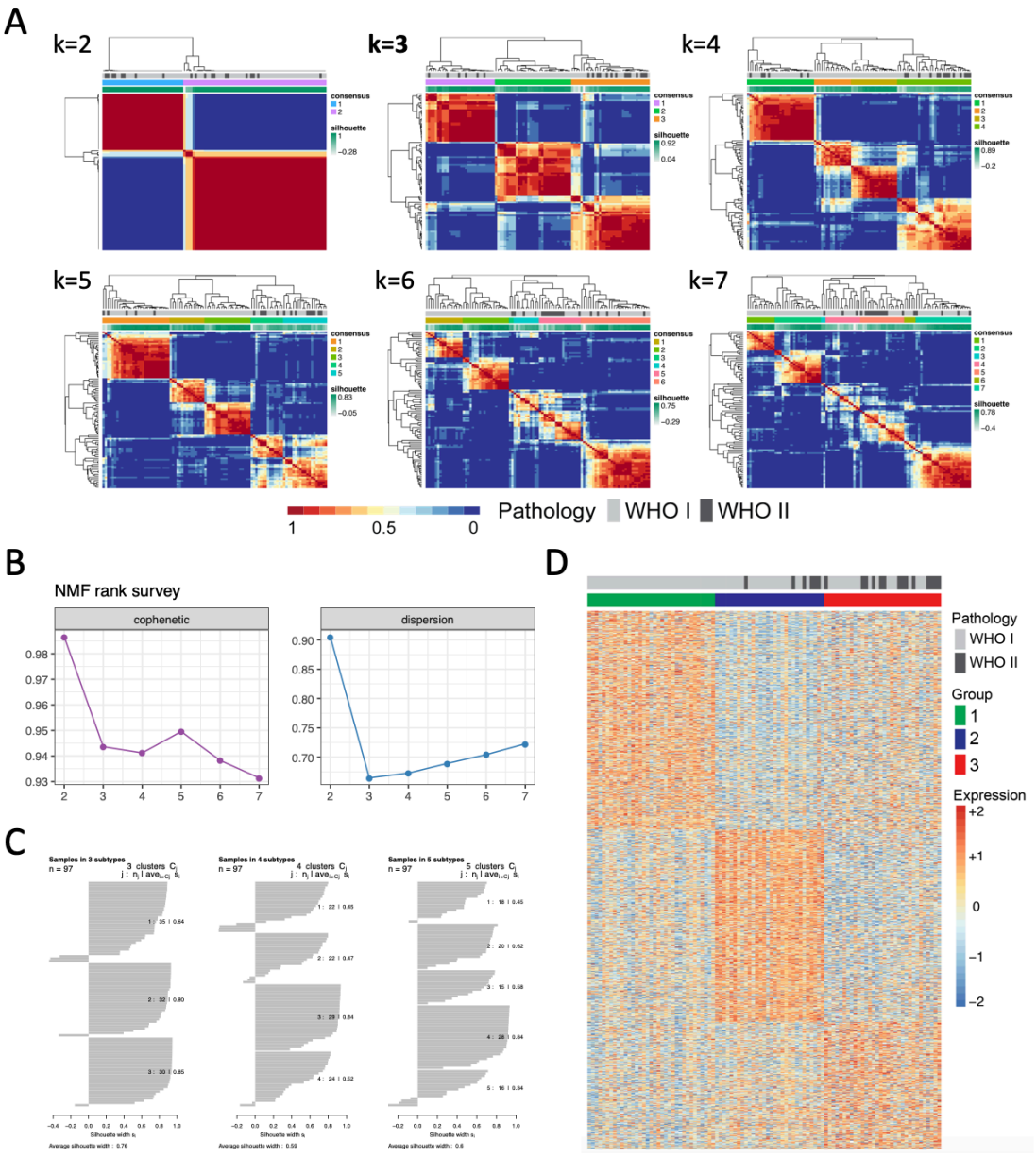

Fig. S1 NMF for rank k=2 to k=7 on the 1500 most variable genes. (**A**) Heatmaps on the consensus matrix shows the average connectivity of the 97 samples from the 1000 runs for each rank. (**B**) Cophenetic correlation coefficients and dispersion associated with clusters observed from each rank. (**C**) Silhouette analysis on clusters observed from rank 3 to 5 shows that k=3 is the optimal number of clusters as all clusters give average silhouette width of greater than 0.6, while there exist clusters lower than 0.5 for other ranks. (**D**) Expression heatmap of the top 1,500 most variable genes in the discovery set. Group 1 is labelled in green; group 2, blue; group 3, red.

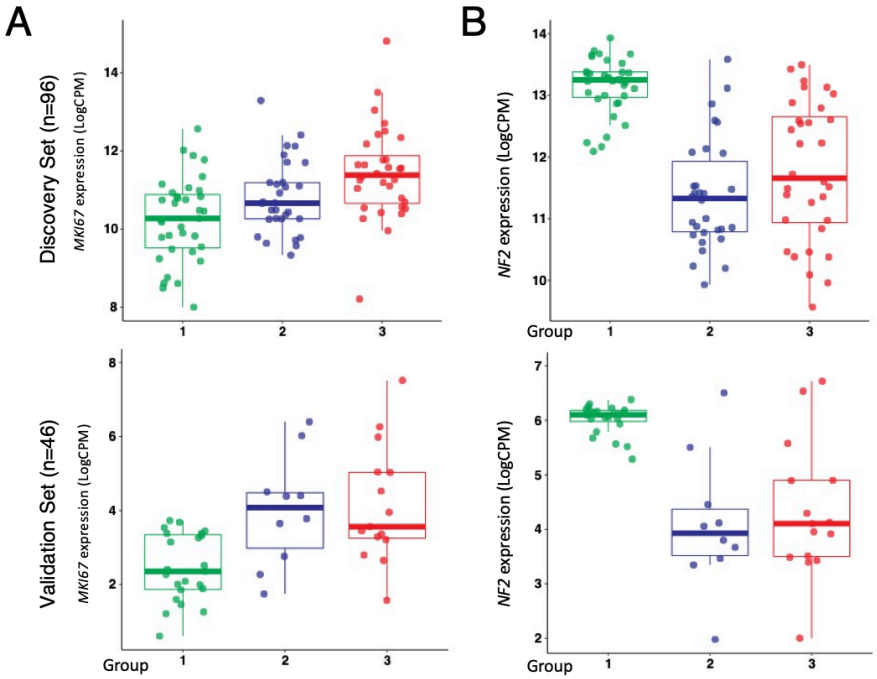

Fig. S2 MKI67 and NF2 expression level by subgroup (**A**) Boxplot demonstrating MKI67 expression for groups 1 to 3 in the discovery set (upper panel) and validation set (lower panel). (**B**) Boxplot showing NF2 expression in each of the three subgroups in the discovery set (upper panel) and validation set (lower panel). NR2 expression between groups 2 and 3 is not statistically different.

Acknowledgements

Portions of this study were funded by the Roderick D. MacDonald Fund, the Jan and Dan Duncan Neurologic Research Institute at Texas Children's Hospital, and the Hamill Foundation. AJP was supported by a K08 award from the NINDS (K08NS102474). HYZ is supported by the Howard Hughes Medical Institute. We would like to acknowledge Vicky Brandt for insightful comments on the manuscript and Kathy Relyea for illustration in Figure 2c.

Contributions

A.J.P. conceived the main study idea; A.J.P and T.J.K. designed and/or performed experiments, analyzed data, and wrote and revised the manuscript. Y.W.W. and Z.L. performed and interpreted computational analyses. J.F.M. performed statistical analysis. J.P.R., M.O. and S.S. performed sample preparation of patient tissue. M.C., L.X., D.M.M., H.D., and D.A.W. performed next generation sequencing experiments. K.A.H. and J.C.G. performed histopathological classification. A.J.P., S.P.G., and D.Y. provided patient samples. A.J., D.A.W., G.R., D.Y., S.E.P., and H.Y.Z. provided feedback on study design, reviewed the data, and revised the manuscript. All authors gave final approval.

Conflict of Interest Sharon E. Plon is a member of the Scientific Advisory Board for Baylor Genetics. Other authors declare no competing interests.

References

1. Ostrom, Q. T. *et al.* CBTRUS Statistical Report: Primary Brain and Central Nervous System Tumors Diagnosed in the United States in 2008-2012. *Neuro. Oncol.* **17**, iv1–iv62 (2015).
2. Wiemels, J., Wrensch, M. & Claus, E. B. Epidemiology and etiology of meningioma. *Journal of Neuro-Oncology* **99**, 307–314 (2010).
3. Pearson, B. E. *et al.* Hitting a moving target: evolution of a treatment paradigm for atypical meningiomas amid changing diagnostic criteria. *Neurosurg. Focus* **24**, E3 (2008).
4. Aghi, M. K. *et al.* Long-term recurrence rates of atypical meningiomas after gross total resection with or without postoperative adjuvant radiation. *Neurosurgery* **64**, 56–60 (2009).
5. Modha, A. & Gutin, P. H. Diagnosis and treatment of atypical and anaplastic meningiomas: A review. *Neurosurgery* **57**, 538–549 (2005).
6. Zaher, A., Abdelbari Mattar, M., Zayed, D. H., Ellatif, R. A. & Ashamallah, S. A. Atypical meningioma: A study of prognostic factors. *World Neurosurgery* **80**, 549–553 (2013).
7. Rogers, L. *et al.* Meningiomas: knowledge base, treatment outcomes, and uncertainties. A RANO review. *J. Neurosurg.* **122**, 4–23 (2015).
8. Verhaak, R. G. W. *et al.* Integrated Genomic Analysis Identifies Clinically Relevant Subtypes of Glioblastoma Characterized by Abnormalities in PDGFRA, IDH1, EGFR, and NF1. *Cancer Cell* **17**, 98–110 (2010).
9. Network, C. G. A. R. Integrated genomic analyses of ovarian carcinoma. *Nature* **474**, 609–615 (2011).
10. Perou, C. M. *+ *et al.* Molecular portraits of human breast tumours. [Letter]. *Nature* (2000). doi:10.1038/35021093
11. Pugh, T. J. *et al.* Medulloblastoma exome sequencing uncovers subtype-specific somatic mutations. *Nature* **488**, 106–110 (2012).
12. Peyre, M. & Kalamarides, M. Molecular genetics of meningiomas: Building the roadmap towards personalized therapy. *Neurochirurgie* (2014). doi:10.1016/j.neuchi.2014.06.007
13. Harmancl, A. S. *et al.* Integrated genomic analyses of de novo pathways underlying atypical meningiomas. *Nat. Commun.* **8**, (2017).
14. Sahm, F. *et al.* DNA methylation-based classification and grading system for meningioma: a multicentre, retrospective analysis. *Lancet Oncol.* **18**, 682–694 (2017).
15. Clark, V. E. *et al.* Genomic analysis of non-NF2 meningiomas reveals mutations in TRAF7, KLF4,

AKT1, and SMO. *Science (80-.).* **339**, 1077–1080 (2013).

16. Clark, V. E. *et al.* Recurrent somatic mutations in POLR2A define a distinct subset of meningiomas. *Nat. Genet.* **48**, 1253–1259 (2016).

17. Brastianos, P. K. *et al.* Genomic sequencing of meningiomas identifies oncogenic SMO and AKT1 mutations. *Nat. Genet.* **45**, 285–289 (2013).

18. Olar, A. *et al.* Mitotic index is an independent predictor of recurrence-free survival in meningioma. in *Brain Pathology* (2015). doi:10.1111/bpa.12174

19. Swiderska, Z. *et al.* Comparison of the Manual, Semiautomatic, and Automatic Selection and Leveling of Hot Spots in Whole Slide Images for Ki-67 Quantification in Meningiomas. *Anal. Cell. Pathol.* **2015**, (2015).

20. Rezanko, T., Akkalp, A. K., Tunakan, M. & Sari, A. A. MIB-1 counting methods in meningiomas and agreement among pathologists. *Anal. Quant. Cytol. Histol.* **30**, 47–52 (2008).

21. Bi, W. L. *et al.* Genomic landscape of high-grade meningiomas. *npj Genomic Med.* **2**, 15 (2017).

22. Cai, D. X. *et al.* Chromosome 1p and 14q FISH analysis in clinicopathologic subsets of meningioma: Diagnostic and prognostic implications. *J. Neuropathol. Exp. Neurol.* (2001). doi:10.1093/jnen/60.6.628

23. Müller, P. *et al.* Deletion of chromosome 1p and loss of expression of alkaline phosphatase indicate progression of meningiomas. *Clin. Cancer Res.* (1999).

24. Kane, A. J. *et al.* Anatomic location is a risk factor for atypical and malignant meningiomas. *Cancer* (2011). doi:10.1002/cncr.25591

25. Subramanian, A. *et al.* Gene Set Enrichment Analysis: A Knowledge-Based Approach for Interpreting Genome- Wide Expression Profiles Gene set enrichment analysis: A knowledge-based approach for interpreting genome-wide expression profiles. *Source Proc. Natl. Acad. Sci. United States Am.* **102**, 15545–15550 (2005).

26. Mootha, V. K. *et al.* PGC-1α-responsive genes involved in oxidative phosphorylation are coordinately downregulated in human diabetes. *Nat. Genet.* **34**, 267–273 (2003).

27. Sadasivam, S. & DeCaprio, J. A. The DREAM complex: Master coordinator of cell cycle-dependent gene expression. *Nature Reviews Cancer* **13**, 585–595 (2013).

28. Von Schimmelmann, M. *et al.* Polycomb repressive complex 2 (PRC2) silences genes responsible for neurodegeneration. *Nat. Neurosci.* **19**, 1321–1330 (2016).

29. Soshnikova, N. & Duboule, D. Epigenetic temporal control of mouse hox genes in vivo. *Science (80-.).* **324**, 1321–1323 (2009).

30. Liu, Y. *et al.* Histone Lysine Methyltransferase Ezh1 Promotes TLR-Triggered Inflammatory Cytokine Production by Suppressing Tollip. *J. Immunol.* (2015). doi:10.4049/jimmunol.1402087

31. Abel, K. J. *et al.* Characterization of EZH1, a human homolog of Drosophila enhancer of zeste near BRCA1. *Genomics* (1996). doi:10.1006/geno.1996.0537

32. Ezhkova, E. *et al.* EZH1 and EZH2 cogovern histone H3K27 trimethylation and are essential for hair follicle homeostasis and wound repair. *Genes Dev.* (2011). doi:10.1101/gad.2019811

33. Ben-Porath, I. *et al.* An embryonic stem cell-like gene expression signature in poorly differentiated aggressive human tumors. *Nat. Genet.* (2008). doi:10.1038/ng.127

34. Vasudevan, H. N. *et al.* Comprehensive Molecular Profiling Identifies FOXM1 as a Key Transcription Factor for Meningioma Proliferation. *Cell Rep.* **22**, 3672–3683 (2018).

35. Mages, C. F., Wintsche, A., Bernhart, S. H. & Müller, G. A. The DREAM complex through its subunit Lin37 cooperates with Rb to initiate quiescence. *Elife* (2017). doi:10.7554/elife.26876

36. Litovchick, L., Florens, L. A., Swanson, S. K., Washburn, M. P. & Decaprio, J. A. DYRK1A protein kinase promotes quiescence and senescence through DREAM complex assembly. *Genes Dev.* (2011). doi:10.1101/gad.2034211

37. Fischer, M., Grossmann, P., Padi, M. & DeCaprio, J. A. Integration of TP53, DREAM, MMB-FOXM1 and RB-E2F target gene analyses identifies cell cycle gene regulatory networks. *Nucleic Acids Res.* (2016). doi:10.1093/nar/gkw523

38. Collord G, Tarpey P, Kurbatova N, Martincorena I, Moran S, Castro M, Nagy T, Bignell G, Maura F, Young MD, Berna J, Tubio JMC, McMurran CE, Young AMH, Sanders M, Noorani I, Price SJ, Watts C, Leipnitz E, Kirsch M, Schackert G, Pearson D, Devadass A, Ram Z, M. U. An integrated genomic analysis of anaplastic meningioma identifies prognostic molecular signatures. *Sci. Rep.* **8**, 13537 (2018).

39. Louis, D. N. *et al.* The 2016 World Health Organization Classification of Tumors of the Central Nervous System: a summary. *Acta Neuropathologica* **131**, 803–820 (2016).

40. Wang, L. *et al.* Genomic profiling of Sézary syndrome identifies alterations of key T cell signaling and differentiation genes. *Nat. Genet.* **47**, 1426–1434 (2015).

41. Love, M. I., Huber, W. & Anders, S. Moderated estimation of fold change and dispersion for RNA-seq data with DESeq2. *Genome Biol.* **15**, (2014).

42. Law, C. W., Chen, Y., Shi, W. & Smyth, G. K. Voom: Precision weights unlock linear model analysis tools for RNA-seq read counts. *Genome Biol.* **15**, (2014).

43. Ritchie, M. E. *et al.* Limma powers differential expression analyses for RNA-sequencing and microarray

studies. *Nucleic Acids Res.* **43**, e47 (2015).

44. Leek, J. T., Johnson, W. E., Parker, H. S., Jaffe, A. E. & Storey, J. D. The SVA package for removing batch effects and other unwanted variation in high-throughput experiments. *Bioinformatics* **28**, 882–883 (2012).

45. Morelandy, R. T., Ryany, J. F., Pan, C. & Baxevanis, A. D. The Homeodomain Resource: A comprehensive collection of sequence, structure, interaction, genomic and functional information on the homeodomain protein family. *Database* **2009**, (2009).

46. Klisch, T. J., Vainshtein, A., Patel, A. J. & Zoghbi, H. Y. Jak2-mediated phosphorylation of Atoh1 is critical for medulloblastoma growth. *Elife* (2017). doi:10.7554/elife.31181